ADVANCES IN ATMOSPHERIC SCIENCES, VOL. 38, JUNE 2021, 1020–1027

• Notes & Letters •

Convective/Large-scale Rainfall Partitions of Tropical Heavy Precipitation in CMIP6 Atmospheric Models

Jing YANG*[1,2], Sicheng HE[1], and Qing BAO[3]

[1]*State Key Laboratory of Earth Surface Process and Resource Ecology/Key Laboratory of Environmental Change and Natural Disaster, Ministry of Education, Faculty of Geographical Science, Beijing Normal University, Beijing* 100875, *China*

[2]*Southern Marine Science and Engineering Guangdong Laboratory, Guangzhou* 511458, *China*

[3]*State Key Laboratory of Numerical Modeling for Atmospheric Sciences and Geophysical Fluid Dynamics (LASG), Institute of Atmospheric Physics, Chinese Academy of Sciences, Beijing* 100029, *China*

(Received 19 July 2020; revised 1 February 2021; accepted 4 February 2021)

ABSTRACT

Convective/large-scale (C/L) precipitation partitions are crucial for achieving realistic rainfall modeling and are classified in 16 phase 6 of the Coupled Model Intercomparison Project (CMIP6) atmospheric models. Only 4 models capture the feature that convective rainfall significantly exceeds the large-scale rainfall component in the tropics while the other 12 models show 50%–100% large-scale rainfall component in heavy rainfall. Increased horizontal resolution generally increases the convective rainfall percentage, but not in all models. The former 4 models can realistically reproduce two peaks of moisture vertical distribution, respectively located in the upper and the lower troposphere. In contrast, the latter 12 models correspond to three types of moisture vertical profile biases: (1) whole mid-to-lower tropospheric wet biases (60%–80% large-scale rainfall); (2) mid-tropospheric wet peak (50% convective/large-scale rainfall); and (3) lower-tropospheric wet peak (90%–100% large-scale rainfall). And the associated vertical distribution of unique clouds potentially causes different climate feedback, suggesting accurate C/L rainfall components are necessary to reliable climate projection.

Key words: CMIP6, heavy precipitation, convective precipitation, moisture vertical distribution

Citation: Yang, J., S. C. He, and Q. Bao, 2021: Convective/large-scale rainfall partitions of tropical heavy precipitation in CMIP6 atmospheric models. *Adv. Atmos. Sci.*, **38**(6), 1020−1027, https://doi.org/10.1007/s00376-021-0238-4.

Article Highlights:

- Large-scale rainfall significantly exceeds the convective component for tropical heavy rainfall in most CMIP6 models.
- The classification of convective/large-scale rainfall components are closely associated with four types of moisture vertical distributions.
- The associated different cloud vertical distributions potentially cause different climate responses and large uncertainties in climate projections.

1. Introduction

Heavy precipitation can cause huge losses in terms of human life, economies, and ecosystems (Meehl et al., 2000; Lesk et al., 2016) and has significantly increased with global warming (Lehmann et al., 2015; Donat et al., 2016). Accurate modeling and prediction of heavy precipitation events are crucial but challenging. Current global climate system models (GCMs) have large biases in modeling tropical precipitation (Li and Xie, 2014; Huang et al., 2018), particularly heavy precipitation (Dai, 2006; He et al., 2019). Unrealistic convective and large-scale precipitation components essentially contribute to the biases of simulated precipitation (Zhang et al., 1994; Gomes and Chou, 2010; Yang et al., 2013). Although sometimes total rainfall amounts can be simulated well, the convective and large-scale precipitation partitions are incorrect in the models (Kyselý et al., 2016). Therefore, the status of convective and large-scale precipitation components in current GCMs needs to be clarified.

Moreover, convective and large-scale precipitation com-

* Corresponding author: Jing YANG
Email: yangjing@bnu.edu.cn

ponents are closely associated with the vertical distribution of moisture (Bretherton et al., 2004) and cloud fractions (Zhao, 2014; Wang and Zhang, 2016). Because the radiative effects of low and high clouds differ (Wetherald and Manabe, 1988), the different components of convective and large-scale precipitation may closely correspond to different climate feedbacks (Zelinka et al., 2013, Stephens et al., 2019), eventually driving uncertainties in climate change projection (Andrews et al., 2012; Kauppinen and Malmi, 2018). Distinguishing the differences in convective and large-scale precipitation among climate models is helpful in understanding the uncertainties of future projection.

The outputs of the new-generation phase 6 of the Coupled Model Intercomparison Project (CMIP6) models were recently released, providing a new opportunity to revisit the aforementioned dilemmas. Are there any distinct features of the convective/large-scale (C/L) precipitation partitions among these CMIP6 models, particularly in terms of heavy rainfall? To what extent does model resolution influence C/L rainfall components in heavy rainfall? And what are the associated moisture/cloud vertical distributions? The following sections will answer the above questions in sequence.

2. Datasets and methodology

The model outputs are retrieved from the newly released CMIP6 models (https://esgf-node.llnl.gov/search/cmip6/), which are shown in Table S1 in the Electronic Supplementary Material (ESM). To simplify the study and avoid the inclusion of air-sea interaction, only the Atmospheric Model Intercomparison Project (AMIP) and HighResMIP Tier 1 runs are chosen (Eyring et al., 2016, Haarsma et al., 2016). Additionally, the selected models need to have released both daily accumulated precipitation and convective precipitation variables, as well as relative humidity (RH) and cloud fraction. The first ensemble member "r1i1p1f1" of most models is used in this study, though some models (CNRM-CM6-1, CNRM-ESM2-1, and UKESM1-0-LL) do not include "r1i1p1f1 " but provide "r1i1p1f2". The time period 2000–14 is used for this study, but the sensitivity of results to using different study periods and different members was examined, showing no major differences (see Figs. S1 and S2 in the ESM).

To identify the effect of horizontal resolution on C/L components, several pairs of models which released both high- and low-resolution versions were obtained (see section 3.2). To identify the climate feedback, the surface air temperature outputs are also applied in the simulations forced by an abrupt quadrupling of CO_2 (*abrupt-4xCO_2*) experiment of CMIP6 models, which covers the years 2000–14. The observed RH is derived from ECMWF Reanalysis v5 (ERA5) (Copernicus Climate Change Service, 2017), which has a horizontal resolution of 0.25° × 0.25° and 37 pressure levels. To avoid the effect of resolution on results, all model datasets were interpolated onto a 1° × 1° grid using the nearest-neighbor interpolation method (Accadia et al., 2003).

To describe the frequency/percentage distribution of precipitation as a function of intensity, the daily precipitation rate was divided into a 1 mm d^{-1} interval, starting from 0.5 mm d^{-1} (He et al., 2019). Following the definition of different precipitation intensities by the China Meteorological Administration and previous studies (e.g., Matsumoto and Takahashi, 1999; He et al., 2019), this study focuses on features above 50 mm d^{-1}, which is the usual threshold selection for heavy precipitation.

A 1 mm d^{-1} interval composite of rainfall intensity for the whole tropical domain was made in order to investigate the behaviors of moisture and cloud fraction vertical profiles against different rainfall intensities. Here, the tropical region covers the area between 20°S and 20°N. To discuss the effect of climate feedback, the surface temperature anomaly of the period 1850–2000 was obtained by removing the air temperature of the year 1850.

3. Convective/large-scale rainfall partition of tropical heavy precipitation in CMIP6

3.1. *Classification of C/L rainfall partitions for tropical heavy rainfall in CMIP6*

To recognize the current status of tropical C/L rainfall partitions associated with heavy rainfall in CMIP6, the frequency distributions and percentage contributions of the C/L component against rainfall intensity in 16 CMIP6 model outputs focusing on heavy rainfall were investigated, as shown in Fig. 1. As a result, only four models in CMIP6 (EC-Earth3, UKESM1-0-LL, HadGEM3-GC31-HM, and SAM0-UNICON) have the feature that convective rainfall exceeds large-scale rainfall in heavy rainfall, as shown in Fig. 1(I). In contrast, in the other 12 models, large-scale rainfall is equal to or exceeds convective rainfall in the heavy rainfall partition as show in Fig. 1(II, III, IV), and those models were further categorized into three major types according to different percentage contributions of C/L rainfall. The first type includes BCC-CSM2-MR, CESM2, NESM3, GFDL-CM4, MIROC6, FGOALS-g3, and MRI-AGCM3-2-H [see Fig. 1(II)]. For these models, the convective rainfall exceeds the large-scale rainfall in intensity at approximately less than 50 mm d^{-1} while it becomes less than the large-scale component at greater than 50 mm d^{-1}, except for MIROC6 which has more convective rainfall until 170 mm d^{-1}. The percentage of the large-scale rainfall is gradually increasing with the intensity increase and reaches approximately 70%–80% in extreme heavy rainfall. The second type includes CNRM-ESM2-1, CNRM-CM6-1, and ECMWF-IFS-HR [see Fig. 1(III)]. For these models, the convective rainfall exceeds the large-scale rainfall at less than 50 mm d^{-1} while the large-scale and convective rainfall nearly account for a similar percentage (50%) for extreme rainfall greater than 50 mm d^{-1}. The third type includes CanESM5

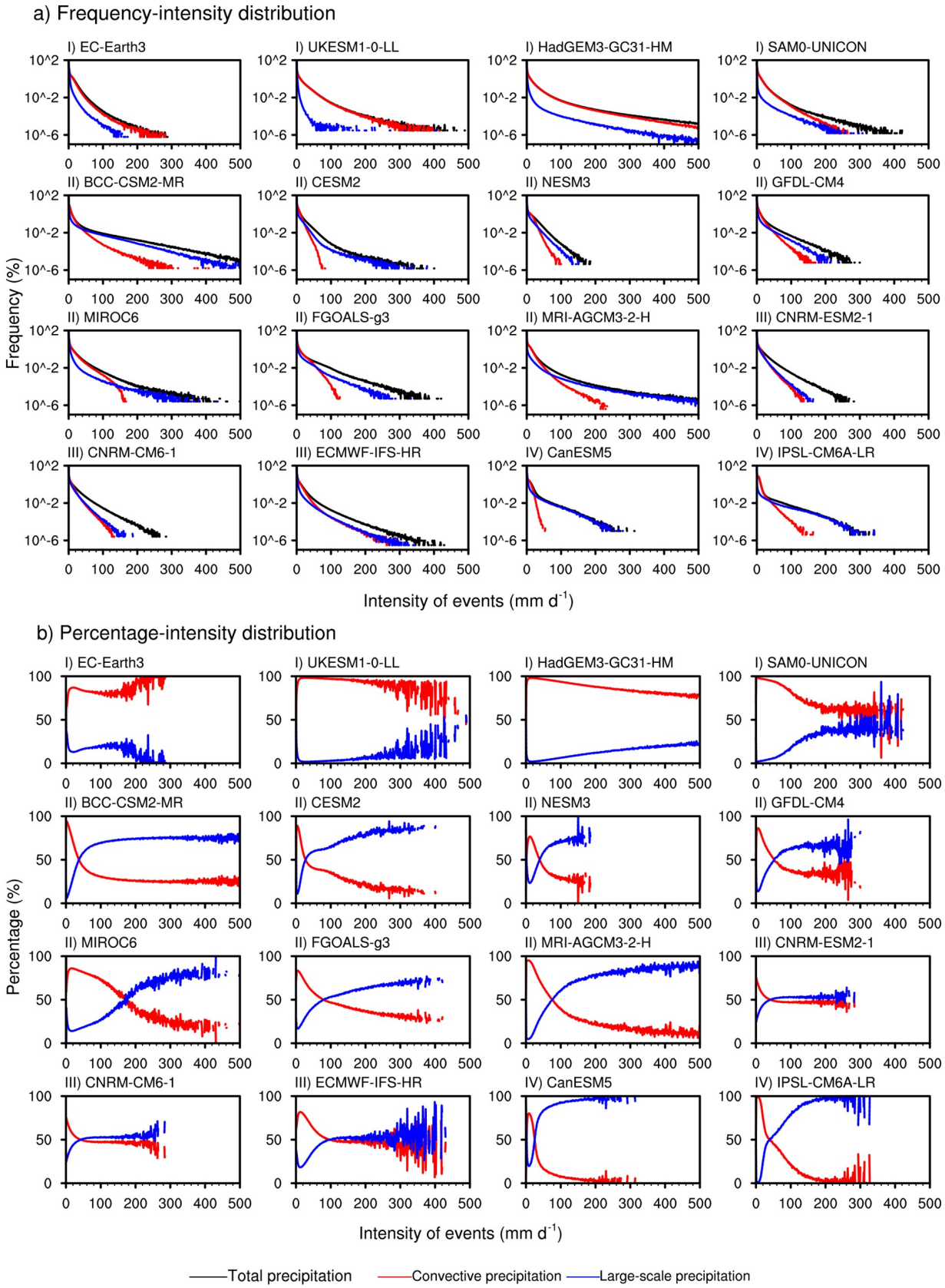

Fig. 1. Frequency–intensity distribution of total (black), convective (red), and large-scale (blue) rainfall (a) and percentage–intensity distribution of large-scale and convective rainfall (b) in CMIP6. I–IV denotes four categories of convective and large-scale precipitation partitions.

and IPSL-CM6A-LR [see Fig. 1(IV)]. For these models, the convective component is greater than the large-scale rainfall for a precipitation intensity less than 50 mm d^{-1} but sharply decreases at greater than 50 mm d^{-1}. The large-scale precipitation falsely increases with increased intensity and contributes nearly 100% for a heavy extreme rainfall greater than 150 mm d^{-1}. In other words, the category I models have much more convective rainfall than large-scale rainfall in heavy rainfall; the category II models have more large-scale precipitation than convective precipitation in heavy rainfall; the category III models have similar percentages of large-scale and convective rainfalls in heavy rainfall; and the category IV models almost only include the large-scale precipitation component in extreme heavy rainfall.

3.2. *How do horizontal resolutions influence C/L partition in CMIP6?*

As previous studies have reported, the partitions of convective and large-scale rainfall may be associated with horizontal spatial resolution (Weisman et al., 1997, Pieri et al., 2015; He et al., 2019). Here, the effect that model horizontal resolution has on the C/L component in CMIP6 is examined through the following two approaches. First, the convective rainfall components between higher and lower versions of some given models are compared. For example, HadGEM-GC3 and IPSL-CM6A are shown in Fig. 2a. In HadGEM-GC3, which features convective rainfall exceeding large-scale rainfall in heavy rainfall, the convective rainfall percentage in its higher resolution (0.23° × 0.35°) is slightly less than that in its lower resolution (1.25° × 1.875°) at intensities between 50 mm d^{-1} and 300 mm d^{-1} but becomes more than that in its lower resolution at intensities greater than 400 mm d^{-1}. However, differing results are found for IPSL-CM6A, which has more large-scale rainfall than convective rainfall in heavy rainfall. Compared with the IPSL-CM6A lower resolution (1.26° × 2.5°) version, the convective percentage in the higher resolution (0.5° × 0.7°) version is greater at intensities less than 300 mm d^{-1} but lower for heavy extreme rainfall greater than 400 mm d^{-1}. In both lower and higher resolution versions of IPSL-CM6A, the first-order feature remains that large-scale rainfall significantly exceeds convective rainfall, which is not influenced by difference in horizontal resolution.

Second, a comparison between two groups of models with relatively lower and higher resolutions (see the model descriptions in Table S2 in ESM) is made, shown in Fig. 2b. The results show that averaged convective rainfall accounts for a larger percentage in the high-resolution group than in the low-resolution group of CMIP6. Meanwhile, the multimodel ensemble convective rainfall percentage exceeds large-scale rainfall in the high-resolution group while large-scale rainfall exceeds convective rainfall in the low-resolution group of CMIP6 at intensities between 50–300 mm d^{-1}. Accordingly, the models with higher resolution generally produce more convective rainfall partition than those with lower resolution. However, not all models follow this trend. Higher resolution does not always lead to higher convective rainfall percentage.

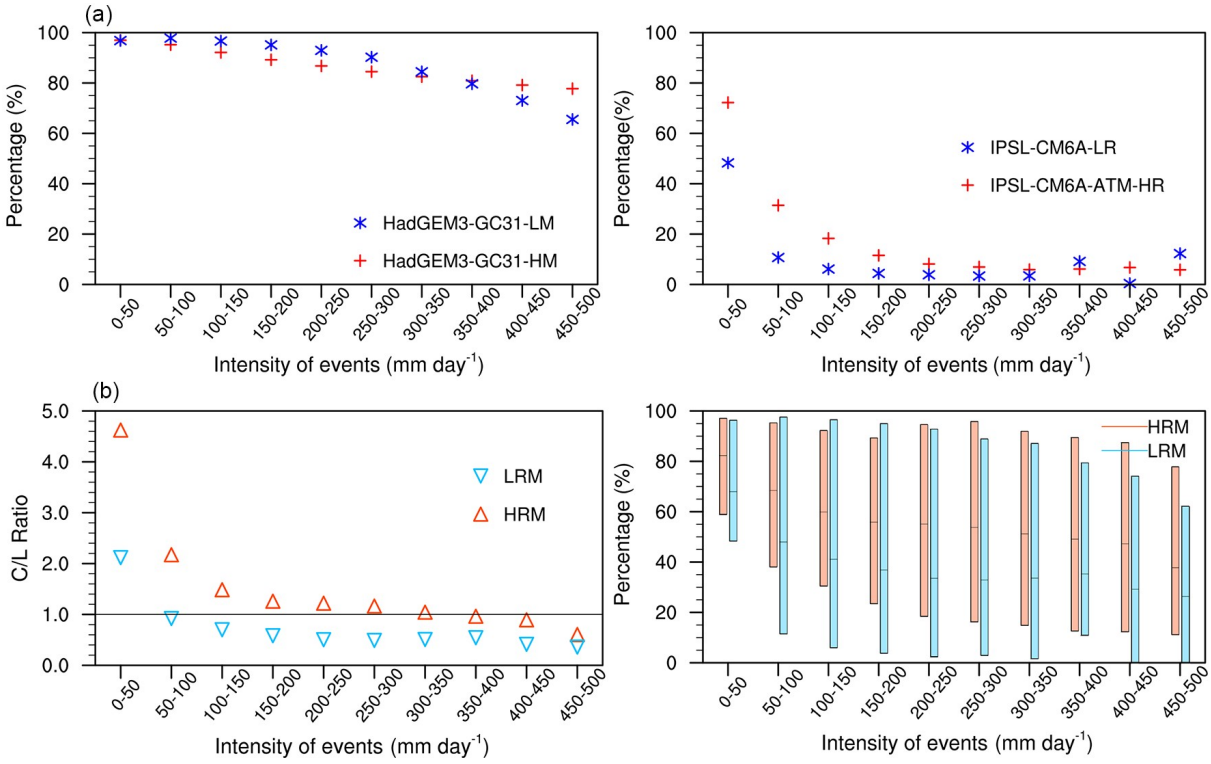

Fig. 2. (a) Convective rainfall percentage of higher (red) and lower (blue) resolution versions in given models and (b) convective rainfall percentage (right panel) and C/L percentage ratio (left panel), respectively in HRM (red) and LRM (blue).

4. Moisture/cloud vertical distributions associated with C/L rainfall components in CMIP6 models and their implications

Previous studies have reported that the vertical distribution of moisture is directly associated with heavy rainfall simulation (Bretherton et al., 2004, He et al., 2019). Meanwhile, the vertical distribution of moisture influences cloud vertical distribution and further affects climate feedback (Zelinka et al., 2013). Therefore, it is necessary to examine the vertical profile of moisture and investigate if there are relevant common features associated with the C/L components. As shown in Fig. 3, there are two peaks of RH located in the upper troposphere (150–200 hPa) and lower troposphere (850–1000 hPa), respectively, under observation. The vertical distribution of moisture against different precipitation intensities averaged in the tropical region is illustrated for 16 CMIP6 models, as shown in Fig. S3 in the ESM. In comparison, a remarkable, common feature of the aforementioned category I models (EC-Earth3, UKESM1-0-LL, SAM0-UNICON, and HadGEM3-GC31-HM) with more convective rainfall is that they can capture the two RH peaks well approximately over the upper and lower troposphere, although the RH peak levels are slightly different.

However, in the other three categories of models, those that have more large-scale than convective precipitation in the extreme rainfall partition, the aforementioned two remarkable peaks of RH vertical distribution under observation are not reproduced well, particularly the upper-level peak. In terms of the three categories based on the different categories of convective/large-scale components mentioned in section 3.1, the associated RH distributions primarily show common biases for each category, as shown in Fig. 3. In cat-

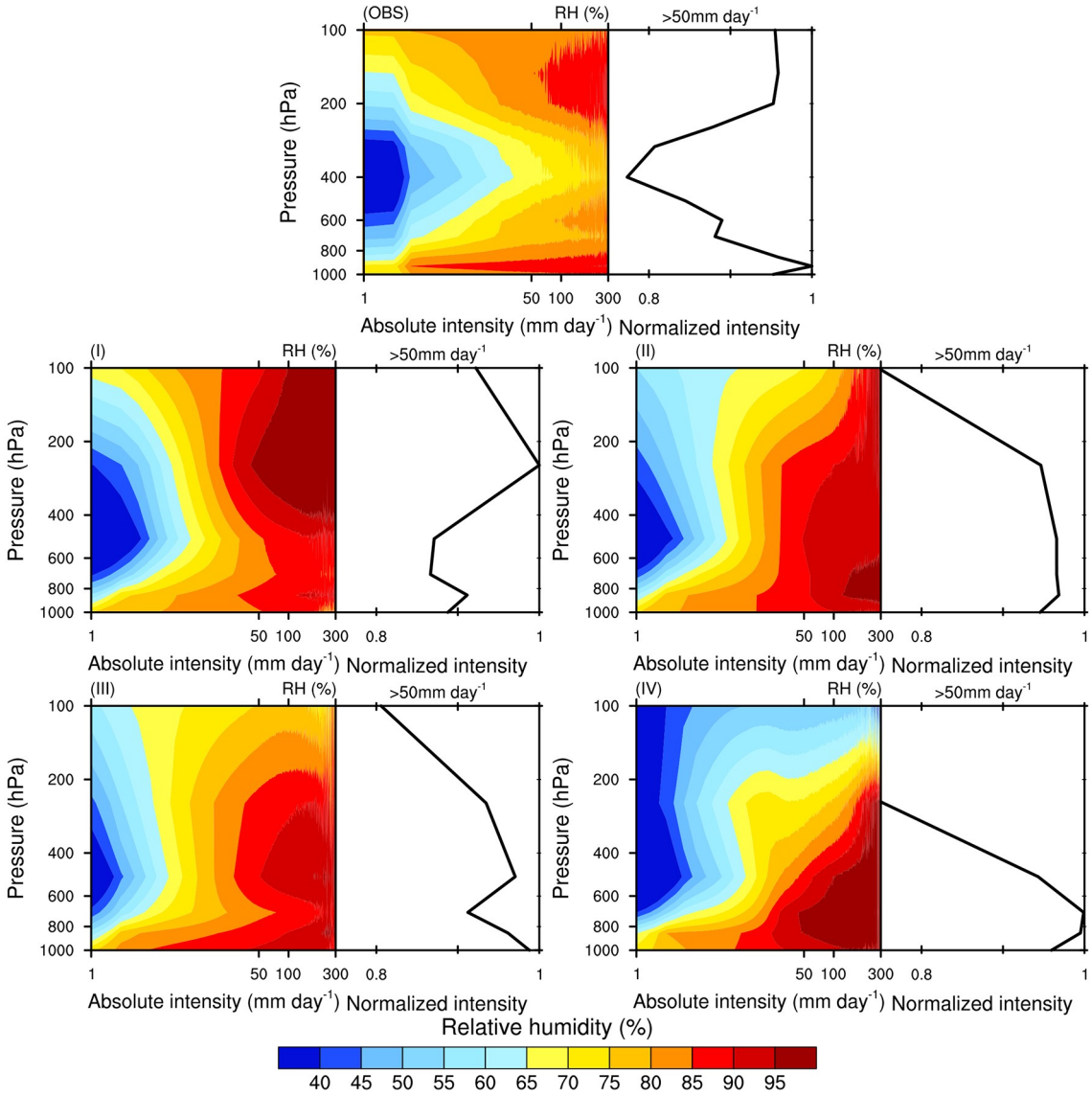

Fig. 3. Composite vertical profiles of RH against different precipitation intensities (contour on the left) and the normalized vertical profile of RH at greater than 50 mm d^{-1} (XY plot on the right) based on GPM/ERA5 and four categories of C/L component in CMIP6.

egory II, the observed RH upper-level peak disappears and the whole middle-lower tropospheric atmosphere is wet below 300 hPa, which corresponds to the large-scale rainfall (the maximum is nearly 80%) exceeding convective rainfall for extreme partition greater than 50 mm d^{-1}, except for MRI-AGCM3-2-H and GFDL-CM4. In category III, the RH upper-level peak is significant but lower and located at over 500 hPa, which corresponds to the comparable C/L rainfall in the rainfall extreme partition. In category IV, in which 100% of the extreme portion precipitation comes from large-scale rainfall and 0% comes from convective rainfall, the observed RH upper-level peak also disappears, and the simulated RH has only a single vertical peak with a large amount of moisture trapped in the lower troposphere, which accordingly causes heavy large-scale rainfall.

In observation, heavy rainfall is typically caused by deep convection in tropical regions, which usually corresponds to cloud tops higher than 15 km (Sekaranom et al., 2018, Fig. 3). Considering the accessible daily cloud vertical distribution output, one model in each category was purposely chosen to examine its cloud vertical distribution as shown in Fig. 4. In category I, the extreme rainfall partition features a large mid-to-high cloud fraction, which is consistent with deep convection. In category II, the cloud fraction between 200 hPa and 700 hPa significantly increases during extreme rainfall, which corresponds to lower cloud tops, an increased middle-to-lower cloud fraction, and increased cloud thickness between 200 hPa and 700 hPa. Therefore, the large-scale rainfall overcomes the convective rainfall in the simulation of this condition. In category III, high clouds

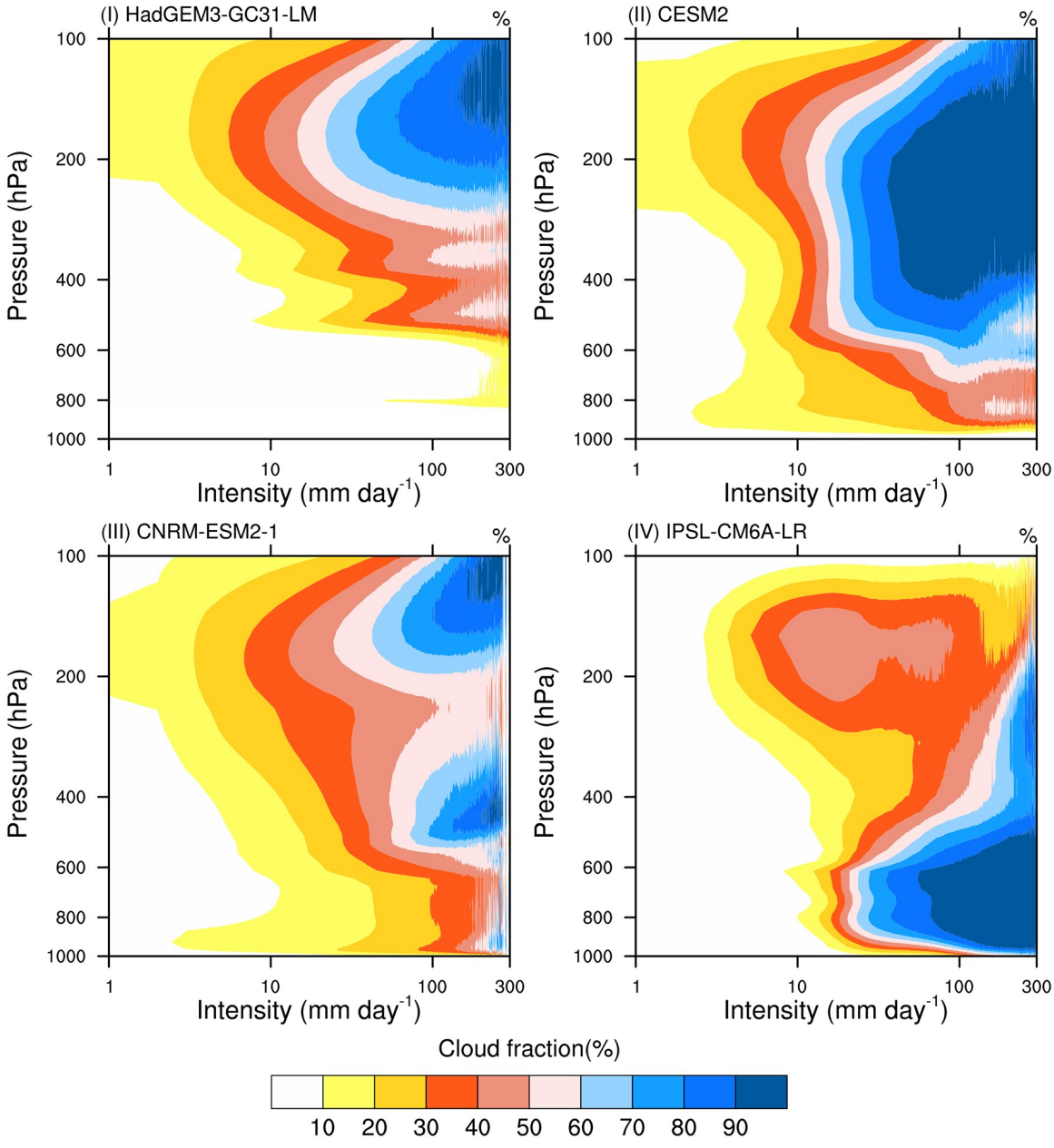

Fig. 4. Composite vertical profiles of cloud fraction based on different precipitation intensities in four CMIP6 models.

at approximately 100–150 hPa and middle clouds at approximately 500 hPa are distinguishable, which corresponds to comparable convective and large-scale rainfalls in the simulation. In category IV, low clouds are dominant, which is consistent with the 100% large-scale rainfall in the extreme rainfall simulation. Because different cloud types have different contributions to climate adjustments in coupled models under global warming (Zelinka et al., 2013), the distinct vertical distributions of the cloud fraction provide the greatest source of intermodal spread in climate response to greenhouse warming, which can be somewhat detected, as shown in Fig. S4 (Soden and Held, 2006; Po-Chedley et al., 2019).

5. Conclusion and discussion

The C/L precipitation partitions are crucial for achieving realistic rainfall modeling. Using newly released CMIP6 model outputs, the convective and large-scale precipitation partitions are comprehensively classified with focus on heavy rainfall that is greater than 50 mm d^{-1}. Only 4 AMIP models (EC-Earth3, UKESM1-0-LL, HadGEM3-GC31-HM, and SAM0-UNICON) capture the feature that convective rainfall significantly exceeds the large-scale rainfall component, while the other 12 models show more large-scale than convective component in heavy rainfall. Further investigation revealed that higher resolution generally produces more convective rainfall, with some exceptions. In terms of associated moisture vertical distribution, the 4 "realistic" models are those that have more convective rainfall components and can realistically reproduce two peaks in moisture vertical distribution, located in the upper (250 hPa) and lower (850 hPa) troposphere. In contrast, the other 12 "unrealistic" models correspond to three types of moisture vertical profile biases. The first type of bias is that between a 60%–80% and 40%–20% partition of large-scale/convective rainfall in the extreme partition corresponds to the unrealistic whole mid-to-lower tropospheric wetness; the second type of bias is that 50% convective/large-scale extreme rainfall corresponds to a false mid-tropospheric (500 hPa) wet peak; and the third type of bias is that large-scale rainfall accounts for nearly 100% of the extreme intensity corresponding to a single evident peak in the lower troposphere. The associated cloud vertical distributions are accordingly distinct, which potentially causes different climate responses to greenhouse emissions and eventually contributes to the greatest uncertainty due to the intermodal spread in climate projection.

Note that it is challenging to find appropriate observations to make an apples-to-apples comparison with a GCM. On one hand, in satellite observations, most stratiform precipitation in the tropics is a precipitation from anvil clouds of a convective system (Tao et al., 2006) and characterized by a "bright band (melting layer)" (Awaka et al., 2007). In GCMs, convective and large-scale precipitations are calculated by a convection scheme and a large-scale condensation scheme, respectively. Therefore, large-scale precipitation in the model is not the same as stratiform precipitation in the satellite observations. On the other hand, the rain intensity in satellite observations is the instantaneous intensity (mm h^{-1}), which may pass through a particular grid point only once in about five days. As the daily average of the rain intensity is a conditional average (average over the rainy area and rainy time only), it does not represent the daily accumulated rain amount (mm d^{-1}) for the grid cell in a GCM. However, the convective rain intensity should be larger than large-scale rain intensity in the tropics (Tao et al., 2010). Heavier large-scale precipitation in the tropics in GCMs may be due to some deficiency of the cumulus parameterization scheme in most models, so that the tropical convective precipitation may be represented by unrealistically heavy large- scale precipitation.

Acknowledgements. This study was supported by funding from the National Natural Science Foundation of China (Grant 42022034, 91737306, 41675100), and National Key Research and development Program of China (Grant No. 2017YFA0604004). We would like to thank Professor Letu HUSI from the Institute of Remote Sensing and Digital Earth of CAS and Professor Qi Liu from the University of Science and Technology of China (USTC) for their useful comments on satellite datasets. We would also like to acknowledge the high-performance computing support from the Center for Geodata and Analysis, Faculty of Geographical Science, Beijing Normal University (https://gda.bnu.edu.cn/). Finally, we would like to thank two anonymous reviewers for their useful comments and suggestions about this study.

Electronic supplementary material: Supplementary material is available in the online version of this article at https://doi.org/10.1007/s00376-021-0238-4.

REFERENCES

Accadia, C., S. Mariani, M. Casaioli, A. Lavagnini, and A. Speranza, 2003: Sensitivity of precipitation forecast skill scores to bilinear interpolation and a simple nearest-neighbor average method on high-resolution verification grids. *Wea. Forecasting*, **18**, 918–932, https://doi.org/10.1175/1520-0434(2003)018,0918:SOPFSS.2.0.CO;2.

Andrews, T., J. M. Gregory, M. J. Webb, and K. E. Taylor, 2012: Forcing, feedbacks and climate sensitivity in CMIP5 coupled atmosphere-ocean climate models. *Geophys. Res. Lett.*, **39**, L09712, https://doi.org/10.1029/2012GL051607.

Awaka, J., T. Iguchi, and K. Okamoto, 2007: Rain type classification algorithm. *Measuring Precipitation from Space: EURAINSAT and the Future*, V. Levizzani et al., Eds., Springer, 213–224, https://doi.org/10.1007/978-1-4020-5835-6_17.

Bretherton, C. S., M. E. Peters, and L. E. Back, 2004: Relationships between water vapor path and precipitation over the tropical oceans. *J. Climate*, **17**, 1517–1528, https://doi.org/10.1175/1520-0442(2004)017<1517:RBWVPA>2.0.CO;2.

Copernicus Climate Change Service (C3S), 2017: ERA5: Fifth generation of ECMWF atmospheric reanalyses of the global climate. Copernicus Climate Change Service Climate Data Store (CDS). [Available from https://cds.climate.copernicus.eu/cdsapp#!/home]

Dai, A. G., 2006: Precipitation characteristics in eighteen coupled climate models. *J. Climate*, **19**, 4605–4630, https://doi.org/10.1175/JCLI3884.1.

Donat, M. G., A. L. Lowry, L. V. Alexander, P. A. O'Gorman, and N. Maher, 2016: More extreme precipitation in the world's dry and wet regions. *Nature Climate Change*, **6**, 508–513, https://doi.org/10.1038/nclimate2941.

Eyring, V., S. Bony, G. A. Meehl, C. A. Senior, B. Stevens, R. J. Stouffer, and K. E. Taylor, 2016: Overview of the coupled model intercomparison project phase 6 (CMIP6) experimental design and organization. *Geoscientific Model Development*, **9**, 1937–1958, https://doi.org/10.5194/gmd-9-1937-2016.

Gomes, J. L., and S. C. Chou, 2010: Dependence of partitioning of model implicit and explicit precipitation on horizontal resolution. *Meteor. Atmos. Phys.*, **106**, 1–18, https://doi.org/10.1007/s00703-009-0050-7.

Haarsma, R. J., and Coauthors, 2016: High resolution model intercomparison project (HighResMIP v1.0) for CMIP6. *Geoscientific Model Development*, **9**, 4185–4208, https://doi.org/10.5194/gmd-9-4185-2016.

He, S. C., J. Yang, Q. Bao, L. Wang, and B. Wang, 2019: Fidelity of the observational/reanalysis datasets and global climate models in representation of extreme precipitation in east China. *J. Climate*, **32**, 195–212, https://doi.org/10.1175/JCLI-D-18-0104.1.

Huang, D. Q., P. W. Yan, J. Zhu, Y. C. Zhang, X. Y. Kuang, and J. Cheng, 2018: Uncertainty of global summer precipitation in the CMIP5 models: A comparison between high-resolution and low-resolution models. *Theor. Appl. Climatol.*, **132**, 55–69, https://doi.org/10.1007/s00704-017-2078-9.

Kauppinen, J., and P. Malmi, 2018: Major feedback factors and effects of the cloud cover and the relative humidity on the climate. [Retrieved from http://arxiv.org/abs/1812.11547]

Kyselý, J., Z. Rulfová, A. Farda, and M. Hanel, 2016: Convective and stratiform precipitation characteristics in an ensemble of regional climate model simulations. *Climate Dyn.*, **46**, 227–243, https://doi.org/10.1007/s00382-015-2580-7.

Lehmann, J., D. Coumou, and K. Frieler, 2015: Erratum to: Increased record-breaking precipitation events under global warming. *Climatic Change*, **132**, 517–518, https://doi.org/10.1007/s10584-015-1466-3.

Lesk, C., P. Rowhani, and N. Ramankutty, 2016: Influence of extreme weather disasters on global crop production. *Nature*, **529**, 84–87, https://doi.org/10.1038/nature16467.

Li, G., and S. Xie, 2014: Tropical Biases in CMIP5 Multimodel Ensemble: The Excessive Equatorial Pacific Cold Tongue and Double ITCZ Problems. *J. Climate*, **27**(4), 1765–1780, https://doi.org/10.1175/JCLI-D-13-00337.1.

Matsumoto, J., and K. Takahashi, 1999: Regional differences of daily rainfall characteristics in East Asian summer monsoon season. *Geographical Review of Japan, Series B.*, **72**, 193–201, https://doi.org/10.4157/grj1984b.72.193.

Meehl, G. A., and Coauthors, 2000: An introduction to trends in extreme weather and climate events: Observations, socioeconomic impacts, terrestrial ecological impacts, and model projections. *Bull. Amer. Meteor. Soc.*, **81**, 413–416, https://doi.org/10.1175/1520-0477(2000)081<0413:AITTIE>2.3.CO;2.

Pieri, A. B., J. Von Hardenberg, A. Parodi, and A. Provenzale, 2015: Sensitivity of precipitation statistics to resolution, microphysics, and convective parameterization: A case study with the high-resolution WRF climate model over Europe. *Journal of Hydrometeorology*, **16**, 1857–1872, https://doi.org/10.1175/JHM-D-14-0221.1.

Po-Chedley, S., M. D. Zelinka, N. Jeevanjee, T. J. Thorsen, and B. D. Santer, 2019: Climatology explains intermodel spread in tropical upper tropospheric cloud and relative humidity response to greenhouse warming. *Geophys. Res. Lett.*, **46**, 13 399–13 409, https://doi.org/10.1029/2019GL084786.

Sekaranom, A. B., E. Nurjani, and I. Pujiastuti, 2018: Cloud structure evolution of heavy rain events from the East-West Pacific Ocean: A combined global observation analysis. *IOP Conference Series: Earth and Environmental Science*, **148**, 012006, https://doi.org/10.1088/1755-1315/148/1/012006.

Soden, B. J., and I. M. Held, 2006: An assessment of climate feedbacks in coupled ocean-atmosphere models. *J. Climate*, **19**, 3354–3360, https://doi.org/10.1175/JCLI3799.1.

Stephens, B. A., C. S. Jackson, and B. M. Wagman, 2019: Effect of tropical nonconvective condensation on uncertainty in modeled projections of rainfall. *J. Climate*, **32**, 6571–6588, https://doi.org/10.1175/JCLI-D-18-0833.1.

Tao, W.-K., and Coauthors, 2006: Retrieval of latent heating from TRMM measurements. *Bull. Amer. Meteor. Soc.*, **87**, 1555–1572, https://doi.org/10.1175/BAMS-87-11-1555.

Tao, W.-K., S. Lang, X. P. Zeng, S. Shige, and Y. Takayabu, 2010: Relating convective and stratiform rain to latent heating. *J. Climate*, **23**, 1874–1893, https://doi.org/10.1175/2009JCLI3278.1.

Wang, Y., and G. J. Zhang, 2016: Global climate impacts of stochastic deep convection parameterization in the NCAR-CAM5. *Journal of Advances in Modeling Earth Systems*, **8**, 1641–1656, https://doi.org/10.1002/2016MS000756.

Weisman, M. L., W. C. Skamarock, and J. B. Klemp, 1997: The resolution dependence of explicitly modeled convective systems. *Mon. Wea. Rev.*, **125**, 527–548, https://doi.org/10.1175/1520-0493(1997)125<0527:TRDOEM>2.0.CO;2.

Wetherald, R. T., and S. Manabe, 1988: Cloud feedback processes in a general circulation model. *J. Atmos. Sci.*, **45**, 1397–1416, https://doi.org/10.1175/1520-0469(1988)045<1397:CFPIAG>2.0.CO;2.

Yang, B., and Coauthors, 2013: Uncertainty quantification and parameter tuning in the CAM5 Zhang-McFarlane convection scheme and impact of improved convection on the global circulation and climate. *J. Geophys. Res.*, **118**, 395–415, https://doi.org/10.1029/2012JD018213.

Zelinka, M. D., S. A. Klein, K. E. Taylor, T. Andrews, M. J. Webb, J. M. Gregory, and P. M. Forster, 2013: Contributions of different cloud types to feedbacks and rapid adjustments in CMIP5. *J. Climate*, **26**, 5007–5027, https://doi.org/10.1175/JCLI-D-12-00555.1.

Zhang, M. H., J. J. Hack, J. T. Kiehl, and R. D. Cess, 1994: Diagnostic study of climate feedback processes in atmospheric general circulation models. *J. Geophys. Res.*, **99**, 5525–5537, https://doi.org/10.1029/93JD03523.

Zhao, M., 2014: An investigation of the connections among convection, clouds, and climate sensitivity in a global climate model. *J. Climate*, **27**, 1845–1862, https://doi.org/10.1175/JCLI-D-13-00145.1.